JET-P(96)28

# Toroidal Rotation in ICRF Heated H-modes on JET

L-G Eriksson, E Righi, K-D Zastrow.

JET Joint Undertaking, Abingdon, Oxfordshire, OX14 3EA, UK.

Preprint of a paper to be submitted for publication in
Plasma Physics and Controlled Fusion

July 1996

## ABSTRACT

The first measurements of toroidal rotation of the bulk plasma during purely Ion Cyclotron Resonance Frequency (ICRF) heated H-modes on the JET tokamak are reported. Substantial toroidal acceleration in the direction of the plasma current occurs at the transition into H-mode. In the present paper the relationship between toroidal rotation and improved confinement of the H-mode is investigated. We conclude that the dominant driving mechanism for toroidal rotation is the ion pressure gradient.

## 1. INTRODUCTION

Two major heating methods are used on the Joint European Torus (JET) tokamak, Neutral Beam Injection (NBI) and Ion Cyclotron Resonance Frequency (ICRF) heating. ICRF heats the plasma while applying very little torque to the plasma. In such a situation the relationship between toroidal rotation and the ion pressure gradient during the H-mode can be more easily investigated. This is all the more important as ICRF-produced H-modes offer an ideal environment where H-modes sustained by high energy fast ions (like $\alpha$ particles on ITER) can be simulated.

It is well known from JET and other tokamaks that the confinement times of thermal energy and toroidal angular momentum with co-injected NBI are about equal under steady state conditions (see for example Kallenbach A. et *al.*, (1991)). For near-perpendicular NBI, however, it is found that the angular momentum confinement time can significantly exceed the thermal energy confinement time (Asakura N. et *al.*, 1993). Also rotation opposite to the plasma current has been reported in balanced NBI heated discharges in L-mode, whereas the plasma was found to rotate parallel with the plasma current with combined balanced NBI and Lower Hybrid Current Drive (LHCD) (Koide Y. et *al.*, 1992). It was concluded that in the first case the torque was due to ripple loss of energetic ions, whereas the LHCD case was explained by the loss of fast electrons. Rotation in the direction opposite to the plasma current has also been observed on TFTR in ICRF heated plasmas (Hsuan H. et *al.*, 1995).

Rotation parallel with the plasma current has previously been observed on JET in the case of ICRF heated L-mode discharges (Eriksson L.-G. et *al.*, 1992). The effects of ICRF heating on H-mode plasmas have been studied on JET only in NBI-dominated discharges, where ICRF heating at the frequency of the fundamental ion cyclotron frequency of H minority ions ($\omega=\omega_{cH}$) was applied in a D plasma at the end of the NBI phase (Stork D. et *al.*, 1987, de Esch H.P.L. et *al.*, 1990, O'Brien DP et *al.*, 1994). In this case application of ICRF resulted in a sharp drop in toroidal angular frequency.

In this paper the first measurements of toroidal rotation during ICRF-only H-modes are reported. The angular frequency of toroidal rotation is measured with a high resolution X-ray

crystal spectrometer. The method used for such measurements is described in detail in Section 2, where its uncertainties and limitations are also discussed. In Section 3 a wide range of JET discharges, all showing different rotational behaviour during ICRF-only H-modes, are described. Observation of toroidal rotation in ICRF-only H-modes now gives us a good picture of the phenomena involved, and in Section 4 the experimental results are given a theoretical interpretation. Finally, in Section 5 the results are summarised and conclusions are drawn.

## 2. INSTRUMENTATION AND MEASUREMENTS

During 1992/93 the interior of the JET vacuum vessel was extensively modified (Bertolini E. and the JET Team, 1994). A new pumped divertor was installed, and the layout of the vessel interior was changed to accommodate it. Consequently the magnetic axis is now typically located 20 to 30 cm above the geometric midplane, depending on the magnetic configuration. Additionally the inner wall has been equipped with new guard limiters.

The toroidal angular frequency of the plasma is measured with a high resolution X-ray crystal spectrometer (Bartiromo R. et *al.*, 1989) that observes the spectrum near the resonance line w of helium-like nickel ($Ni^{+26}$) (Hsuan H. et *al.*, 1987, Bombarda F. et *al.*, 1988). The line of sight of the instrument is located in the geometric midplane of the torus, as shown in Fig.1, and therefore about 20 to 30 cm below the magnetic axis.

The installation of the inner wall guard limiters has resulted in a partial vignetting in the spectrum, since the impact parameter of the line of sight with respect to the torus axis is wavelength dependent. For the main part of the spectrum the line of sight intersects the plasma twice. However for some wavelengths the line of sight is directed at the guard limiter, which results in the photon count being halved. Additional vignetting is caused at the edges of the spectrum by structures in the neutral beam duct.

Because of these problems caused by the structural changes of the vacuum vessel, the methods developed to derive ion temperature and rotation frequency from the spectra up to medium (Bombarda F. et *al.*, 1989) and high temperature (Zastrow K.-D. et *al.*, 1991) can no longer be used. It must also be noticed that the observed changes in the frequency of toroidal rotation are intrinsically small. It is therefore justified to analyse in detail the procedure used to obtain measurements of toroidal rotation from the observed spectrum, and discuss the uncertainties involved.

### 2.1 Treatment of the spectrum and error evaluation

A new least squares fit program has been developed that, among other things, takes into account the electron temperature dependent apparent shift and broadening of the resonance line due to n>2 dielectronic satellites (Bitter M. et *al.*, 1981). The weighted least squares fit also gives the errors of the fit parameters (Press W.H. et *al.*, 1992). For the data presented in this

paper the statistical error on the frequency of toroidal rotation is about 2-3 krad/sec. The resonance line is described as the real part of the complementary error function with complex argument, the so-called Voigt function, with a Gauss contribution to describe the Doppler broadening and a Lorentz contribution to account for the natural line width and the instrumental function. This function is implemented using the approximations described by Humlícek J. (1982), since this is more than a factor 20 faster than the accurate function described by Gautschi W. (1970). The method is correct to better than $10^{-5}$ of the central intensity over the full line profile.

The atomic data necessary to describe the full structure of the resonance line and its dielectronic satellite lines are taken from Bombarda F. et *al.* (1988) and Zastrow K.-D. et *al.* (1990). Five parameters describe the structure of the resonance line, namely continuum level, resonance line intensity, Doppler width and shift of the resonance line and an effective electron temperature to describe the dielectronic satellite structure. To avoid errors due to the partial vignetting the fit is only performed for channels that are unaffected (see Fig.2). The accuracy of this procedure can be checked by comparing the relative intensity of the satellites that results from this analysis with the expected value from line of sight integrated synthetic spectra based upon the measured electron temperature profile and assuming coronal equilibrium. To avoid the influence of the vignetting the spectrum is truncated in the analysis at a wavelength where there is still a contribution from the satellites. Therefore the measured intensity ratio is always lower than the predicted one. The trend of the measurement and the prediction in time are however in good agreement.

The results of the spectrum analysis represent the plasma conditions in an emission shell of effective minor radius $\langle\rho\rangle$ and width $\sigma(\rho)$, defined as,

$$\rho_N = \frac{1}{2\pi}\int_{R_0}^{R_{wall}} \rho^N \frac{f(Ni^{+26};R)\cdot n_e^2(R)\cdot \varepsilon_w(R)\cdot R}{\sqrt{R^2 - R_0^2}} dR, \qquad N = 0,1,2$$

$$\langle\rho\rangle = \frac{\rho_1}{\rho_0} \tag{1}$$

$$\sigma(\rho) = \sqrt{\frac{\rho_2}{\rho_0} - \langle\rho_1\rangle^2}$$

where $\varepsilon_w(R)$ is the emissivity of the resonance line, $n_e(R)$ is the electron density profile, $R_0$ is the position of the magnetic axis, and $f(Ni^{+26};R)$ is the fraction of helium-like nickel calculated from the electron temperature profile assuming coronal equilibrium (Zastrow K.-D. et *al.*, 1991, Zastrow K.-D. et *al.*, 1990). This position is time dependent, mainly since the magnetic axis moves vertically, but also due to changes in electron temperature. Thus the rotation data

represent, in principle, different points on the radial profile at different times. For the discharges considered in this paper we find that $<\rho>\approx 0.35\pm0.05$ and $\sigma(\rho)\approx 0.15\pm0.05$.

The parallel component of the toroidal velocity $v_\phi$ of an ion emitting radiation of wavelength $\lambda_0$ at a major radius R along the line of sight with a distance of closest approach to the torus axis $R_0(\lambda)$ is $v_\parallel = v_\phi R_0(\lambda)/R$. This movement in the parallel direction will cause a Doppler shift of the observed spectrum $\Delta\lambda/\lambda_0 = -v_\parallel/c$. The angular frequency of toroidal rotation is $\omega = v_\phi/R$, and can therefore be calculated from the observed Doppler shift as $\omega = -c\Delta\lambda/\lambda_0 R_0(\lambda)$. The convention is that the angular frequency is positive for rotation in the same direction as the toroidal plasma current. Any poloidal rotation would result in additional line broadening, since the line of sight intersects the plasma twice in the radial direction.

For the X-ray crystal spectrometer the spectral dispersion as function of the measured position x on the detector is in second order (n=2),

$$n\lambda = 2d\sin\left(\cos^{-1}\left(\cos\theta_0 + \frac{(x - x_0)}{2R_L}\right)\right), \tag{2}$$

where 2d is the lattice constant (=4.000 Å for Ge440) and $2R_L$=25.04m is the diameter of the Rowland circle. Without Doppler shift, the observed spectral line would be seen at the detector coordinate $x_0$ at a Bragg angle $\theta_0$. The wavelength $\lambda_0$ =1.5886 Å for the resonance line of helium-like nickel (Hsuan H. et *al.*, 1987, Bombarda F. et *al.*, 1988) corresponds to a Bragg angle $\theta_0$ =0.91786 rad. The impact parameter of the line of sight, $R_0(\lambda)$, is given by,

$$\begin{aligned} R_0(\lambda) &= R_0(\lambda_0) + \frac{L_0}{\sin\theta_0}(\cos\theta - \cos\theta_0) \\ &= R_0(\lambda_0) + \frac{L_0}{2R_L\sin\theta_0}(x - x_0) \end{aligned} \tag{3}$$

where $L_0$=24.38m is the distance from the crystal to the point of closest approach of the line of sight to the torus axis. The impact parameter of the line of sight for wavelength $\lambda_0$ can be calculated from the major radius of the guard limiter, $R_V$=1.82m, that causes the vignetting for wavelengths larger than $\lambda_V$ at a detector position $x_v$.

The wavelength scale is calibrated by comparison of the derived angular frequency during NBI obtained with visible charge exchange recombination spectroscopy of $C^{+6}$ and corrected for cross section effects (Danielsson M. et *al.*, 1992, von Hellermann M.G. et *al.*, 1995). Fig.3 shows the comparison of the angular frequency of $Ni^{+26}$ with that for $C^{+6}$ at the position $\rho=<\rho>$ (see Eq.(1)) of the emission shell of helium-like nickel. The uncertainty of the absolute level is 10 krad/sec.

The errors on the measurement of the toroidal rotation frequency can then be summarised as follows. The statistical error is about 2-3 krad/sec for the data presented in this paper. The

uncertainty of the absolute level, determined by cross calibration with rotation measurements of carbon, is 10 krad/sec. The electron temperature dependent shift of the resonance line due to dielectronic satellites is included.

### 2.2 Rotation differences between Nickel and Deuterium on JET

According to a neoclassical theory (Kim Y.B., Diamond P.H., and Groebner R.J., 1991) there is a difference between the rotation frequency of nickel (and carbon) and that of deuterium, due to the ion density and temperature gradients, and the presence of a parallel electric field. The theory is applicable to JET, since the background ions are in the banana regime. Depending on the amount of impurities present, different correction factors apply. On JET the case $\alpha = \frac{n_{imp}}{n_{fuel}} \frac{Z_{imp}^2}{Z_{fuel}^2} << 1$, where the impurity viscous force is negligible, applies to nickel, while $\alpha \approx 1$ is valid for carbon. In the first case the correction is proportional to the ion temperature scale length, whilst in the second case there is an additonal term proportional to the ion density scale length. A further correction term is in principle necessary for positions close to the magnetic axis, due to the presence of the toroidal electric field. However this latter term has only been calculated in (Kim Y.B., Diamond P.H., and Groebner R.J., 1991) without viscous damping, and should therefore be used with caution.

All three terms predict that the rotation speed of the impurities is smaller than that of the background plasma, for rotation defined in the direction of the plasma current, as long as temperature and density profiles are peaked.

Differences in angular frequency between nickel and deuterium have been evaluated for the experimental conditions relevant to this paper ($R_0$=2.95 m, a=0.95 m, $I_p$=3 MA, $Z_{eff}$=2.5) and are shown in Fig.4. For the calculation $T_i(r) = T_e(r)$ and $n_{Ni}(r) \propto n_e(r)$ have been assumed, while the toroidal electric field has been estimated from the Spitzer resistivity. All three correction terms are found to be of the order of 2-3 krad/sec, which is comparable with the statistical error of the measurement discussed in Section 2.1.

The theory also predicts a difference of the order of 2 krad/sec between an impurity like carbon ($\alpha \sim 1$) and nickel ($\alpha << 1$), which has an effect on the calibration presented above. Nickel is predicted to rotate slower than deuterium for all radii, since the ion temperature profile is peaked. Towards the edge there is an additional drag on carbon, so that the predicted difference is larger. In the centre however the effect changes sign due to the hollowness of the density profile. The predicted difference between nickel and carbon however is much smaller than the errors in the calibration itself.

Assuming profile shapes to be similar a larger correction would apply for smaller tokamaks, due to the reduction in major radius, minor radius and plasma current, in agreement with results published by the DIII-D Team (Kim J. et *al.*, 1994). Note, however, that already

on DIII-D ($R_0$=1.68m, a=0.62m, $I_p$=1 MA) this correction is only of the order of 10 krad/sec in the plasma centre, and becomes larger only in the vicinity of the last closed flux surface.

## 3. RESULTS

Measurements of toroidal rotation have been obtained during ICRF-only heated L- and H-modes in the 1994/95 JET Experimental Campaign using the technique described in Section 2. Such measurements are particularly interesting since for the first time it is possible to investigate changes in angular momentum frequency $\omega$ and angular momentum density $\ell$ of toroidal rotation correlated with plasma phenomena like the transition to H-mode and giant ELMs. The angular momentum density is defined as $\ell = n_e < m > \theta\omega$, where $n_e$ is the plasma density, <m> is the mean mass per electron, while $\theta$ is the moment of inertia of the flux surface at which the measurement is taken.

Different rotational behaviours of the H-mode plasma have been observed. A typical example of a rotating RF-only H-mode is given by the 2.8T/3MA plasma of Fig.5, where the ICRF heating was used with a predominantly symmetric spectrum peaked around $n_\phi$=30 ($0\pi0\pi$ or dipole phasing, see for example Gormezano C. et *al.*, (1996)). Concomitant with the application of ICRF heating is a small positive (i.e., in the same direction of the plasma current) step in angular frequency (and angular momentum density) in the L-mode phase. This step is real, as observed previously by Eriksson L.-G. et *al.* (1992). During the L-mode phase both $\omega$ and $\ell$ remain constant, but when the L-H transition occurs the plasma starts to accelerate (Fig.6). In the example of Fig.5, like in many other cases, neither $\omega$ nor $\ell$ reach a saturation level, but keep increasing throughout the RF phase. The maximum level reached corresponds to about 10-20% of the rotation observed with NBI in similar experimental conditions ($P \cdot \tau_E \approx 3MW \cdot sec$).

It is well known that neutrals at the plasma edge affect the rotation. This effect is most clearly seen in a series of discharges affected by high recycling levels, of which Fig.7 is an example. In this 3.2T/2.5MA plasma, heated by ICRF with $0\pi\pi0$ phasing, the increased level of charge exchange neutrals from the plasma facing components of the first wall clearly acts as a braking term on the plasma. Thus after the initial acceleration of the plasma, due to the transition to H-mode, the rate of change of both angular momentum density, $d\ell/dt$, and of angular frequency, $d\omega/dt$, first come to a halt, and then reverse sign. This example underlines the role that the level of recycling has on toroidal rotation. This is all the more important in view of the consequences that decreased rotation may have on confinement and plasma stability.

Another notable example is given in Fig.8 (a 3T/3MA plasma with $0\pi0\pi$ phasing of the ICRF wave), where the influence on toroidal rotation of the penetrating giant ELM is evident. In fact in this pulse the plasma starts to accelerate at the H-mode transition, but when the giant

ELM occurs the plasma loses momentum, returning to a value of $\omega$ (and $\ell$) only slightly above that of the L-mode. When the perturbation is dispersed the plasma starts to accelerate again.

As it can be seen in Fig.5, the change in the $D_\alpha$ signal at the L-H transition is relatively small. It is unlikely that the accompanying small change in recycling can explain the increase in rotation velocity. We must therefore look for alternative explanations, which will be discussed in the next Section.

## 4. DISCUSSION

In order to qualitatively interpret our results we need to briefly discuss the theoretical background for plasma rotation. According to neo-classical theory a plasma with an ion pressure gradient will rotate in the direction of the plasma current (Hazeltine R.D. and Meiss J.D., 1992). Normally there are discrepancies between the prediction of neo-classical theory and experimental measurements of plasma rotation (Connor J.W. et *al.*, 1987). These discrepancies can be attributed to presence of neutrals in the plasma and other processes leading to anomalous viscosity. However, the basic driving mechanism described by neo-classical theory remains valid. Thus, if no other momentum sources were present the plasma would rotate in the direction of the plasma current. This is consistent with the observed initial rotation of the plasma and the subsequent acceleration after the L-H transition, when the charge-exchange neutrals are reduced and the pressure gradient builds up.

A radial electric field could, in principle, arise because of thermal ion losses and cause the plasma to rotate toroidally. Indeed rotation opposite to the plasma current is observed in the limiter phase of the discharge, with rotation frequencies up to -40 krad/sec. During the X-point phase, however, the thermal ion losses are reduced, and the plasma slows down to a value that, within the errors of the measurement, is around zero.

### 4.1 Momentum absorption from the RF wave

The situation described above is complicated by the fact that the ICRF waves can act as source of momentum for the plasma. As the resonating ions absorb the wave energy they also absorb momentum from the wave. This is true even if the toroidal wave number spectrum is symmetric, which was the case in the experiments reported in Section 3 ($0\pi0\pi$, $0\pi\pi0$ phasings). In order to see this it is necessary to discuss the nature of the wave particle interaction in more detail.

The discussion will concentrate on the interaction between trapped ions and the waves, since these interactions play a crucial role for the momentum absorption. The geometry of the ion cyclotron resonance absorption in a torus is shown in Fig.9, where the directions of the magnetic field and plasma current are relevant to the experiments reported here. In the vicinity of a point where the Doppler shifted wave frequency equals the cyclotron frequency $\omega_{ci}$ , or a

harmonic of it, resonance interaction takes place, i.e. in a vicinity of $\omega - \vec{k}\cdot\vec{v}_D = n\omega_{ci}$, where $\vec{k}$ is the wave vector (of components $k_{||}$, $k_\perp$ parallel and perpendicular to the external magnetic field, respectively), and $\vec{v}_D$ is the drift velocity (including the parallel velocity of the ion). As a result of the interaction the velocity of the ion is changed (Stix T.H., 1975). This change is mainly in the perpendicular velocity component and to lowest order in $k_\perp\rho$,

$$\Delta v_\perp \propto |E_+| \exp(i\alpha) \ , \tag{4}$$

where $\rho$ is the Larmor radius, $E_+$ is the component of the wave electric field rotating in the direction of the ions and $\alpha$ is the relative phase of the Larmor rotation of the wave as the ion enters the interaction region. However, the parallel velocity has also changed. In fact it can be shown that (Stix T.H., 1975),

$$\Delta v_{||} = k_{||} v_\perp \Delta v_\perp / (n\omega_{ci}) \ . \tag{5}$$

Thus, provided that the wave has a finite parallel wave number, an ion will receive a change in its toroidal velocity $\Delta v_\varphi = \Delta v_{||} B_\varphi / B$. It is now tempting to think that the total change in parallel velocity is zero for a symmetric spectrum, i.e. for $\vec{E}_N = \vec{E}_{-N}$, where $N \approx k_{||} R$ is the toroidal mode number and,

$$\vec{E} = \sum_N \vec{E}_N \exp(iN\varphi) \ . \tag{6}$$

This is, however, not the case. To understand this the radial movement of the ions must be considered. In between the resonant interactions the ions move essentially along unperturbed orbits given by the equilibrium magnetic field. Hence, the canonical angular momentum, $P_\varphi = mRv_\varphi + Ze\psi_p$, where $\psi_p$ is the poloidal flux, is conserved in between interactions. For a trapped particle, the change in parallel velocity at a resonance can then be related to the change in poloidal flux at the turning point, where $v_\varphi = 0$ (see e.g. Chen L., Vaclavik J, and Hammet G. (1988)),

$$\Delta\psi_{p,t.p.} = \frac{mR}{Ze}\Delta v_\varphi \ , \tag{7}$$

where t.p. indicates the turning point. Alternatively, using $\psi_p = \int RB_p dr$, and consistently with the sign conventions of Fig.9,

$$\Delta r_{t.p.} = \frac{m}{ZeB_p}\Delta v_\varphi \ . \tag{8}$$

Absorption of the wave power is a diffusive process in phase space, i.e. a particle must lose its phase information through collisions (Stix T.H., 1975) or non-linear processes (Helander P. and Lisak M., 1992), between successive transits of the resonance region. Thus in Eq.(4) $\alpha$ is random for an ensemble of particles entering a resonance region. Consequently, a particle has equal probability of receiving a positive or negative change of its toroidal velocity. However, because the density of fast resonating ions initially decreases with minor radius there is an effective diffusive flow of fast ions outwards and the sum of the changes in toroidal velocity is finite, i.e. on average $\Delta r_{t.p.}$ is positive. As the fast ion distribution function evolves in time the situation becomes more complicated and the density profile of fast ions might even become hollow (Hellsten T., 1989), but there still is an effective outward flow of fast ions (i.e. ions with high perpendicular velocities) which must be balanced by an inward flow of low energy ions (Hellsten T., 1989) (note that due to a sign error, the direction of the predicted RF torque is wrong in this reference). Consequently, the resonating ions continue to absorb momentum from the wave until a steady state is reached. Thus, the absorption of wave momentum by fast ions for a symmetric spectrum depends on the outward flow of these ions. The momentum absorbed from the wave is transferred to the background plasma via collisions and through a $\vec{J}_r \times \vec{B}$ force, where $\vec{J}_r$ is a radial current in the bulk plasma. This radial current arises in response to the fast ion current, and ensures that charge neutrality is approximately maintained (Hinton F.L. and Robertson J.A., 1984).

The direction of the absorbed momentum can be derived as well. As can be seen from Eq.(8) a net outward flow of fast ions corresponds to a net input of momentum in the direction opposite the current, which is consistent with the direction of the $\vec{J}_r \times \vec{B}$ force on the background plasma. Thus, the total momentum absorbed from the wave and transferred to the background plasma is counter to the plasma current.

With an asymmetric wave spectrum wave momentum can be injected in either direction. Furthermore, the amount of momentum transferred can be significantly higher that in the symmetric case. In reality the wave spectrum is not completely symmetric even when $0\pi0\pi$ or $00\pi\pi$ phasings are used. One of the reasons for this is that the currents in the antenna straps cannot be controlled to 100%. However we do not think that these "intrinsic" asymmetries are large enough to influence the results presented in this paper.

In addition to absorb wave momentum, the resonating ions can also provide a momentum source if they are lost to the wall. The resulting torque from such losses is counter to the plasma current. This effect is fairly weak in JET, where energetic resonating ions are normally well confined. However such an effect could be important in tokamaks where fast ion losses are significant. This is a possible explanation for the counter rotation observed in ICRF heated plasmas on TFTR (Hsuan H. et *al.*, 1995).

### 4.2 Discussion of experimental results

Since the observed rotation is in the direction of the plasma current and it was shown in Section 4.1 that RF induced torque is counter to $I_p$, then it appears that the ion pressure gradient $\nabla p_i$ is the driving mechanism for toroidal rotation. If this is the case, then the angular momentum density is expected to correlate well with $\nabla p_i$. Furthermore, since the ion pressure gradient and the ion pressure itself are closely related, a good correlation with the ion pressure ($\sim n_i T_i$) in the central part of the plasma is also expected.

From the analysis of the spectra, the ion temperature $T_i$ at $\rho \approx <\rho>$ is obtained. The total ion density $n_i$ can be inferred from the local measurement of the electron density and the line average $Z_{eff}$, which is dominated by carbon (Z=6),

$$n_i = n_d + n_C = n_e\left(1 - \frac{Z_{eff} - 1}{Z}\right) . \qquad (9)$$

The local angular momentum in the toroidal direction for times after the L-H transition from all the RF-only H-modes considered in this paper is plotted against the product $n_i T_i$ in Fig.10, which shows that the angular momentum density increases with ion pressure for low recycling conditions (points of low $D_\alpha$ intensity in the figure). This can also be seen in Fig. 11, which shows the time evolution of both angular momentum $\ell$ and $n_i T_i$, normalized to the value at the L-H transition, for the discharge of Fig.5 (32411). From Fig.11 it can be concluded that both quantities evolve on a time scale comparable to the energy confinement time.

This result, together with the fact that the experimentally observed changes in rotation velocity are positive, that is in the same direction as the plasma current, lead us to conclude that the ion pressure gradient plays a dominat role in ICRF-only H-modes, and that consequently the ICRF-induced counter torque must be relatively weak. Furthermore, an increase in ion pressure seems to be sufficient to explain the observed changes in angular momentum density. Although a change in angular momentum confinement is expected at the LH transition, it cannot be clearly demonstrated with our present data.

Lastly, it should be noted that previous results obtained on JET with ICRF heating in L-mode plasmas (Eriksson L.-G. et *al.*, 1992) showed a correlation between rotation and perpendicular energy of the fast ions. In the light of the results presented in this paper, it appears that such correlation cannot be taken as indication of a torque associated with the fast ions.

## 5. SUMMARY AND CONCLUSIONS

In the present paper the first measurements of toroidal rotation during purely ICRF heated H-modes on JET have been reported. The technique used for these measurements has been

described in detail, the absolute error has been established to be of the order of 10 krad/sec, while the statistical error is estimated at 2-3 krad/sec. The X-ray crystal spectrometer measures the rotation velocity of $Ni^{+26}$ impurities. However in Section 2 it has been shown also that for JET plasmas the difference of rotation between $Ni^{+26}$ and D ions is of the order of 2-3 krad/sec at $\rho \equiv <\rho>$, well within experimental error, and that therefore for all practical effects they are the same.

Various examples of rotating H-modes have been introduced. The changes in angular frequency $\omega$ and angular momentum $\ell$ have also been shown to be closely related to the presence of neutrals at the plasma edge. This means that in the presence of high recycling the angular momentum density $\ell$ may not increase. This may have profound consequences on confinement and stability of the plasma in both L- and H-mode conditions, and it will be investigated in detail in the next JET Experimental Campaign.

The contribution of a symmetric RF wave spectrum to toroidal rotation has been found to be in the direction opposite to that of the plasma current. However both theoretical considerations and experimental evidence lead us to conclude that the ion pressure gradient is the main driving mechanism for toroidal rotation, which occurs in the same direction as the plasma current, and that the counter torque produced by RF must be rather small.

## ACKNOWLEDGEMENTS

The authors would like to acknowledge C Gormezano and J Jacquinot for their encouragement, P R Thomas for valuable comments on the paper, D Start, P Helander and T Hellsten for many long and useful discussions, and B Viaccoz for ensuring the reliable operation of the X-ray crystal spectromenter since its installation in JET.

## REFERENCES

Asakura N., Fonck R.J., Jaehnig K.P., Kaye S.M., LeBlanc B., and Okayabashi M. (1993), Nuclear Fusion, **33**, 1165.

Bartiromo R., Bombarda F., Giannella R., Mantovani S., Panaccione L., and Pizzicaroli G. (1989), Rev. Sci. Instr, **60**, 237.

Bertolini E. and the JET Team (1994), Proc. 18th SOFT, Karlsruhe.

Bitter M., von Goeler S., Hill K.W., Horton R., Johnson D., Roney W., Sauthoff N., Silver E., and Stodiek W. (1981), Phys. Rev. Letters **47**, 921.

Bombarda F., Giannella R., Källne E., Tallents G.F., Quant J. (1989), Spectrosc. Radiat. Transfer **41**, 323.

Bombarda F., Giannella R., Källne E., Tallents G.F., Bely-Dubau F., Faucher P., Cornille M., Dubau J., and Gabriel A.H. (1988), Phys. Rev. **A37**, 504.

Chen L., Vaclavik J. and Hammet G. (1988), Nucl. Fusion **28**, 389.

Connor J.W., Cowley S.C., Hastie R.J. and Pan L.R. (1987), Plasma Physics and Controlled Fusion **29**, 919.

Danielsson M., von Hellermann M.G., Källne E., Mandl W., Morsi H.W., Summers H.P. and Zastrow K.-D. (1992), Rev. Sci Instrum **63**, 2241.

Eriksson L.-G., Giannella R., Hellsten T., Källne E. and Sundström G. (1992), Plasma Physics and Controlled Fusion, **34**, 863.

de Esch H.P.L. et *al.* (1990), Proc. 17th EPS Conference on Controlled Fusion and Plasma Physics, Amsterdam, Vol.14B, p. I-90.

Gautschi W. (1970), SIAM J. Numer. Anal. **7**, 187.

Gormezano et *al.* (1996), to be submitted for publication in Nucl. Fusion.

Hazeltine R.D. and Meiss J.D. (1992), *Plasma Confinement*, FIP Vol.86, Addison Wesley, NY.

Helander P. and Lisak M. (1992), Physics of Fluids B **4**, 1927.

Hellsten. T. (1989), Plasma Physics and controlled Fusion **31**, 1391.

von Hellermann M.G., Breger P., Frieling J., König R., Mandl W., Maas A. and Summers H.P. (1995), Plasma Physics and Controlled Fusion **37**, 71.

Hinton F.L. and Robertson J.A. (1984), Phys. Fluids **27**, 1243.

Hsuan H., Bitter M., Hill K.W., von Goeler S., Grek B., Johnson D., Roney W., Sauthoff N., Silver E., and Stodiek W. (1987), Phys. Rev. **A35**, 4280.

Hsuan H. et *al.* (1995), Proc 11th Topical Conference on Radio Frequency Power in Plasmas, Palm Springs, CA.

Humlícek J. (1982), J. Quant. Spectrosc. Radiat. Transfer **29**, 437.

Kallenbach A., Mayer H.-M., Fussmann G., Mertens V., Stroth U., Vollmer O., and the ASDEX Team (1991), Plasma Physics and Controlled Fusion, **33**, 595.

Kim J., Burrell K.H., Gohil P., Groebner R.J., Kim Y.B., St. John H.E., Seraydarian R.P. and Wade M.R. (1994), Phys. Rev. Letters **72**, 2199.

Kim Y.B., Diamond P.H. and Groebner R.J. (1991), Phys. Fluids **B3**, 2050.

Koide Y., Tuda T., Ushigusa K., Asakura N., Sakasai A., Ide S., Ishida S., Kikuchi M., Azumi M., Funahashi A. and the JT60 Team (1992), Proc. 14th Internationl Conf. Plasma Physics and Contr. Nuclear Fusion, Vol 1, p. 777.

O'Brien D.P. et *al.* (1994), Proc. 21st EPS Conference on Controlled Fusion and Plasma Physics, Montpellier, Vol.18B, p.I-346.

Press W.H., Teukolsky S.A., Vetterling W.T. and Flannery B.P. (1992), *Numerical Recipes*, Cambridge University Press, 2nd Edition, p. 665 ff.

Stix, T.H. (1975), Nucl. Fusion **15**, 737.

Stork D. et *al.*(1987), Proc 14th EPS Conference on Controlled Fusion and Plasma Physics, Madrid, Vol.11D, p.I-306.

Zastrow K.-D., Morsi H.W., Danielsson M., von Hellermann M.G., Källne E., König R.T.W., Mandl W., and Summers H.P. (1991), J. Appl. Phys, **70**, 6723.

Zastrow K.-D., Källne E., and Summers H.P. (1990), Phys. Rev. **A41**, 1427.

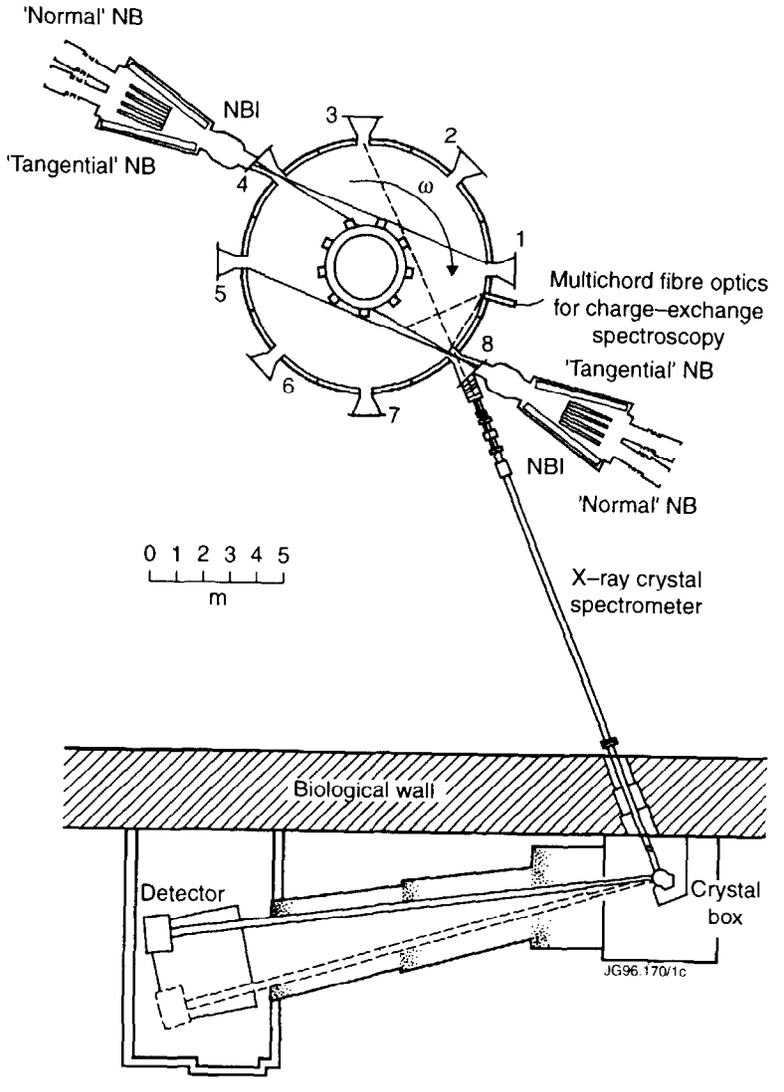


*Figure 1: Layout of the High resolution X-ray crystal spectrometer in the JET vacuum vessel. The position of the Neutral Beam Ducts is also shown.*

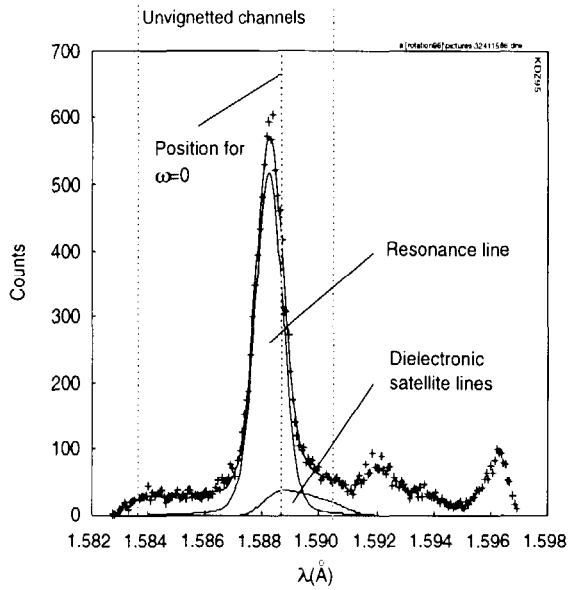


*Figure 2: Spectrum of the resonance line of helium-like nickel taken with the high resolution X-ray crystal spectrometer (JET Pulse No 32410 at t=18.57-18.60). The data are fitted in the unvignetted part of the spectrum, i.e. between the first and last vertical lines. The intermediate vertical line marks the position of the line without Doppler shift. The observed wavelength shift corresponds to a frequency of toroidal rotation of 18 krad/sec.*

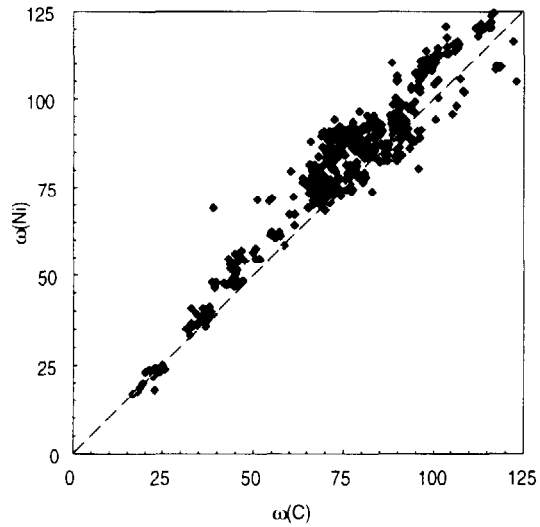


*Figure 3: Comparison under steady-state conditions of toroidal angular frequency measurements of $C^{+6}$ and $Ni^{+26}$ at the same value of <ρ> (see Eq.(1)).*

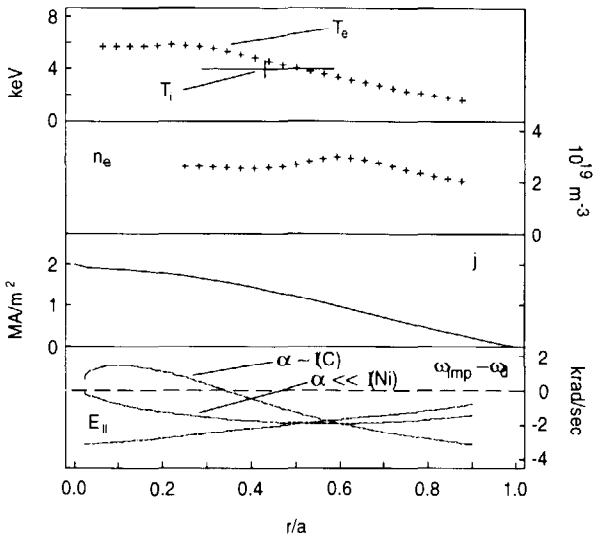


*Figure 4: Input data and results for the calculation of the difference between the rotation frequency of impurities and deuterium for r/a<0.9 (data correspond to the pulse of Fig.5 at t=18.5 sec). In Fig.4a is shown the electron temperature profile from ECE and the single point ion temperature measured with the X-ray crystal spectrometer, showing the position and width of the emission shell (see Eq.(1)). In Fig.4b the electron density profile from LIDAR is reported, while in Fig.4c the toroidal current density calculated from EFIT is shown. The correction terms estimated using the results of Kim Y.B., Diamond P.H. and Groebner R.J. (1991) are shown in Fig.4d for trace impurities (α<<1), dominant impurities (α=1) and for the difference due to the toroidal electric field for nickel.*

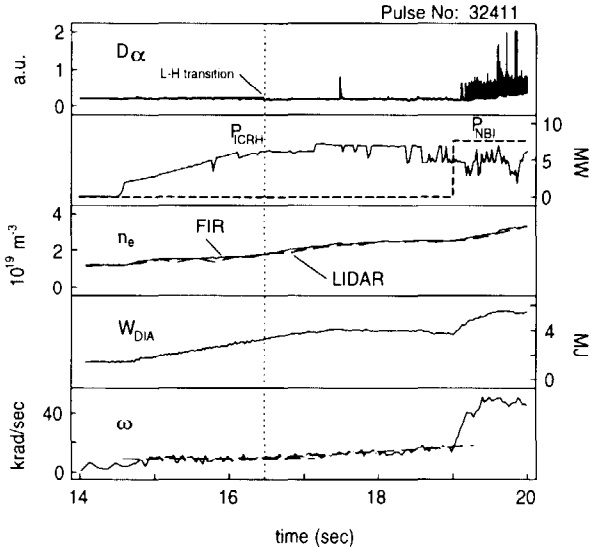


*Figure 5: Example of ELM-free ICRF heated H-mode obtained at $B_t$=2.8T and $I_p$=3MA. At the transition to H-mode the plasma starts to accelerate in the same direction as the plasma current (positive increase in the figure). Note also the different levels of angular frequency between ICRF and NBI: on average it has been estimated to be about 10-20%.*

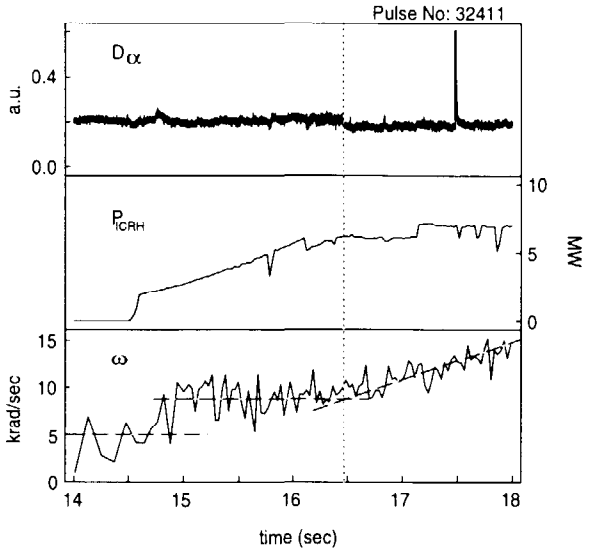


*Figure 6: Close-up of Figure 5 around the H-mode transition. In the figure three phases are evident, corresponding to changes in angular frequency. In the first, Ohmic phase, the angular frequency is around 5 krad/sec. When ICRF is switched on, ω settles around values of 9 krad/sec. Lastly, after the H-mode transition the plasma accelerates in the direction of the plasma current.*

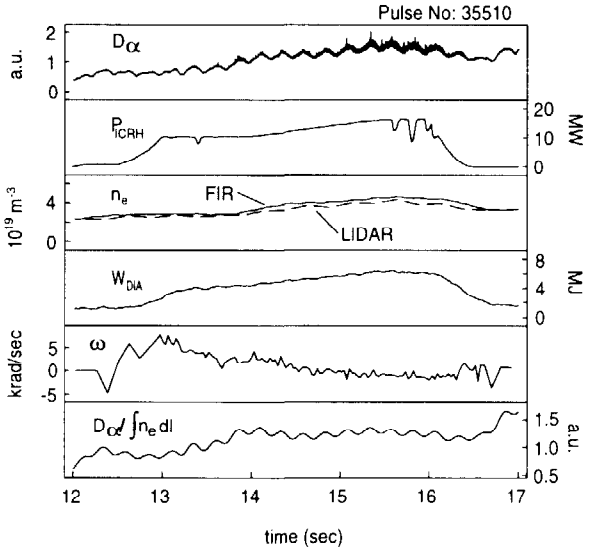


*Figure 7: Increased recycling, expressed as the ratio of the $D_\alpha$ signal and the line integrated density along the same line of sight, during an ICRF heated H-mode ($B_t$=3.2T, $I_p$=2.5MA) causes the plasma to decelerate. At the same time the ELMy nature of the H-mode changes (cfr. with ELM-free H-mode of Fig.5).*

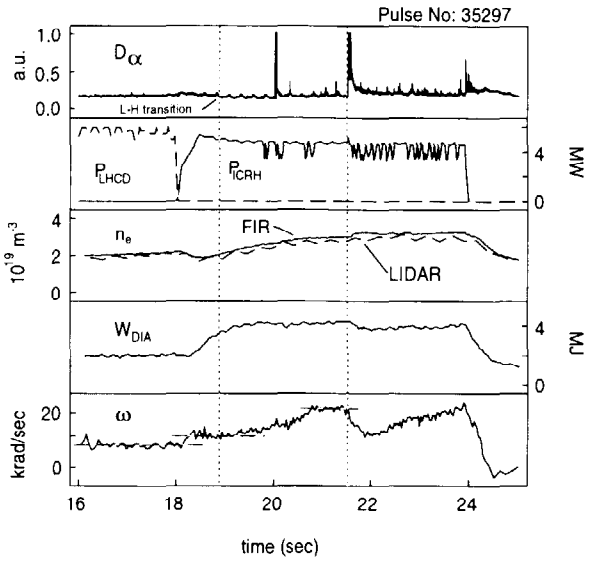


*Figure 8: The effect that edge conditions have on toroidal rotation of the plasma are most clearly seen in this 3T, 3MA H-mode, where the giant ELM perturbs the plasma as deep as $<\rho>\cong 0.35$ causing a sudden deceleration. When the perturbation is dispersed, the plasma accelerates again, eventually reaching values of the angular frequency of the same order of that measured before the giant ELM.*

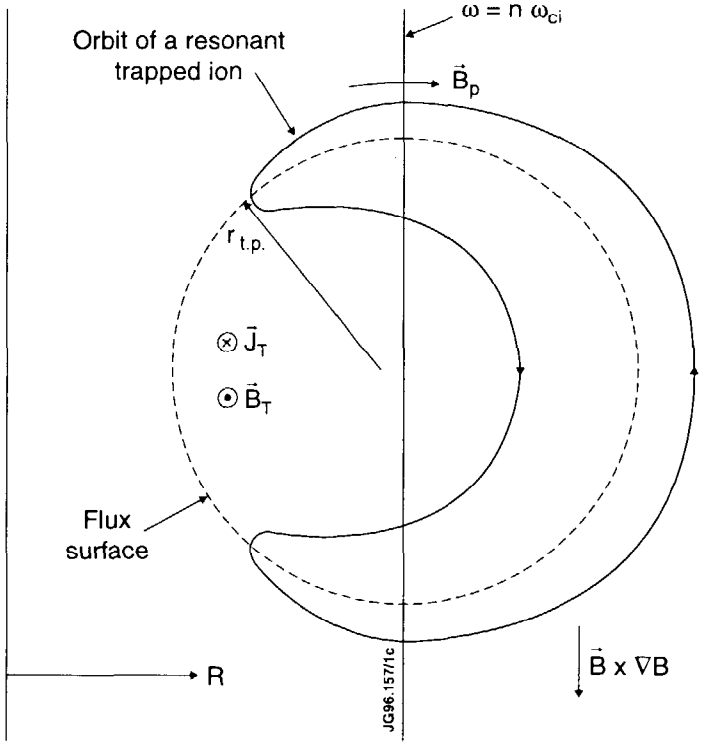


*Figure 9: Geometry of ion cyclotron absorption in a torus. The directions of the magnetic field and current are relevant to the experiments reported in the present paper.*

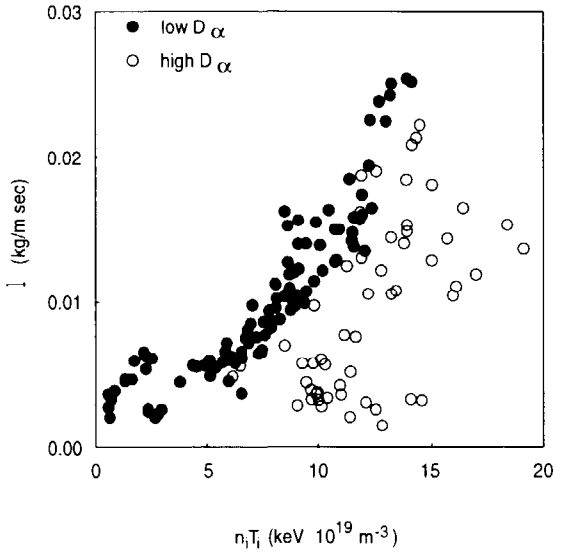


*Figure 10: Correlation between the local angular momentum density and the ion pressure, expressed as the product of ion density and ion temperature, measured at the same radius as $\ell$ ($\rho \equiv <\rho>$). Open circles represent data with high levels of $D\alpha > 4\ 10^{13}/cm^2\ sr\ sec$, filled circles on the other hand represent low recycling conditions.*

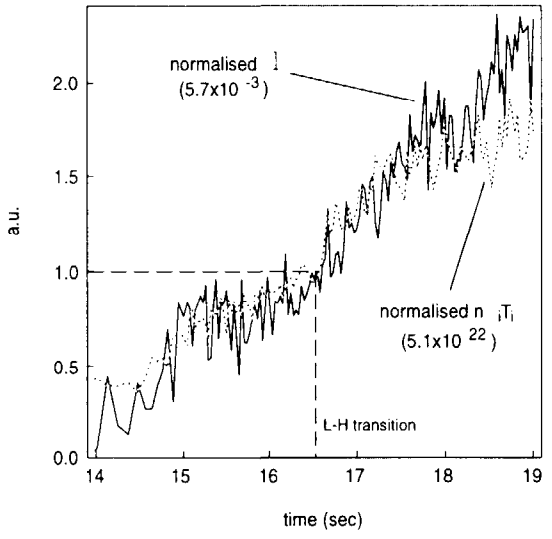


*Figure 11: Time evolution of the local angular momentum density and the ion pressure, expressed as the product of ion density and ion temperature, measured at the same radius as $\ell$ ($\rho \equiv <\rho>$), for pulse 32411 (Fig.5). The data have been normalised to the respective value at the time of the L-H transition.*